J. Fluid Mech. (1991), *vol.* 226, *pp.* 319–347
Printed in Great Britain

The stability of an air film in a liquid flow

By A. M. LEZZI AND A. PROSPERETTI
Department of Mechanical Engineering, The Johns Hopkins University, Baltimore, MD 21218, USA

(Received 12 September 1989 and in revised form 24 October 1990)

A number of processes in which air is entrained in a flow appear to involve the formation of a thin air film between a relatively fast liquid stream and a region of slow recirculation. Eventually, the film breaks into bubbles. This study addresses a possible mechanism causing this process. The linear stability of a vertical film of a viscous gas bounded by liquid in uniform motion on one side, and by liquid at rest on the other side, is studied. Instabilities are found that, depending on the parameter values of the undisturbed flow, are controlled by two basic mechanisms. One is due to the velocity jump across the film and can be related to the usual Kelvin–Helmholtz instability. The second one is controlled by the viscosity jump across the air–liquid interfaces. The relation between the remainder of the discrete spectrum and the spectrum of other parallel shear flows bounded by solid or free surfaces is also discussed.

1. Introduction

The entrainment of air in a flow is an important process very frequently encountered. The ecological balance of water bodies, from small lakes to entire oceans, is critically dependent on the amount of dissolved oxygen. Aeration is a standard technique of water treatment. Furthermore, the formation and detachment of bubbles is an inherently noisy process to which much of the oceanic ambient noise over a large frequency range from hundreds of Hz to many tens of kHz can be ascribed. In spite of this widespread occurrence, not much seems to be known about the basic mechanisms by which entrainment takes place. In a paper devoted to air entrainment in a wave breaking in the spilling mode, Longuet-Higgins & Turner (1974) mention the 'over-running of air by the advancing front' of water and the 'self-aeration' of thin, highly turbulent flows which develops when the turbulent boundary layer on the bottom reaches the surface. While certainly correct and adequate for the purposes of their study, these statements are rather vague as to the precise nature of the process. A literature search has not produced much more detailed information than this. In the present paper we wish to investigate theoretically a possible mechanism by which air can be entrained in flows. Although not the only one, this mechanism appears to be of sufficiently widespread occurrence to warrant its investigation.

A consideration of several examples of entraining flows suggests that a possible mechanism involves the development and instability of a thin air film at the boundary between two liquid currents. The clearest example of this process is offered by a jet falling into a liquid pool. In a high-viscosity liquid an air film surrounding the jet can be clearly discerned for several diameters below the free surface (Lin & Donnelly 1966). The film develops a wavy structure, the amplitude of which

increases with depth, until it breaks up into bubbles. In a low-viscosity liquid such as water the film is more unstable and therefore extends for a shorter distance, but a similar process takes place (figure 1, courtesy of Professor J. Duncan). (In a case such as this one surface waves on the falling jet, due e.g. to turbulence, may also develop. Since the air film is very thin, when these waves reach the surface of the receiving liquid they may close and break off the air film. A similar process may occur in the case of air entrainment by a wave breaking in a plunging mode or by large splashes.)

A detailed flow visualization of air entrainment in a small-scale spilling breaking wave (Banner & Cato 1988), also shows an air film separating the liquid at the face of the wave from the toppling mass forming the recirculating 'toe' of the breaker. A high-speed movie taken from above shows the film to become unstable and to give rise to bubbles that remain entrained in the recirculating liquid mass falling down the face of the wave. This mechanism is possibly similar to the trapping of air occurring in the roller zone of a hydraulic jump (Rajaratnam 1967).

As a third example one may cite the formation of an air film in the form of a 'skirt' at the rim of a gas bubble rising in a liquid (Guthrie & Bradshaw 1969; Hnat & Buckmaster 1976). This film separates the incoming liquid stream from the recirculating flow in the bubble's wake. If the viscosity of the liquid is high, the skirt is well developed and stable. Its thickness has been measured (Guthrie & Bradshaw 1969) and has been found to be of several tens of μm. A similarly stable skirt accompanying spherical-cap bubbles in water is not seen, but even a casual observation shows that small gas bubbles are entrained in the wake of a large spherical-cap bubble, and it is conceivable that they are due, at least in part, to the rapid formation and unstable breakup of a short skirt similar to that found in the high-viscosity case.

In all the above examples the gas film appears at the boundary between a relatively fast liquid stream and a slower flow, typically of a recirculating nature if viewed in a suitable frame. A rather steep velocity change therefore occurs across the thin air film, and one may suspect that the basic mechanism that gives rise to the standard Kelvin–Helmholtz instability could also provide an explanation for the breakup of the film. This was our expectation at the beginning of the study. As it turned out, we have indeed found an instability that can be related to the Kelvin–Helmholtz one. However, this mechanism may be much less important than the instability associated with the jump in viscosity at the interfaces. The possibility of such an instability was first pointed out in the long-wavelength approximation by Yih (1967), who considered plane Couette–Poiseuille flow of two superposed fluid layers between horizontal walls. More recently, Hooper & Boyd (1983, 1987) extended that work to arbitrary wavelengths for the Couette case, and Hinch (1984) proposed a physical explanation of the underlying mechanism. Further extensions have been provided by Renardy (1987), who studied a three-layer vertical Poiseuille flow bounded by solid surfaces, and by Joseph, Renardy & Renardy (1984) and Renardy & Joseph (1985), for configurations with cylindrical symmetry. Since none of these analyses is adaptable to our case, we also develop an explicit treatment of this instability suitable for our situation.

As an attempt to describe the process of air entrainment, this paper is certainly incomplete. In the first place, we ignore the process by which the film is formed. Secondly, the thickness of the film enters as an adjustable parameter in our analysis. Conceivably, an understanding of the mechanism of formation of the film would also predict this quantity. Thirdly, viscous effects are very incompletely accounted for,

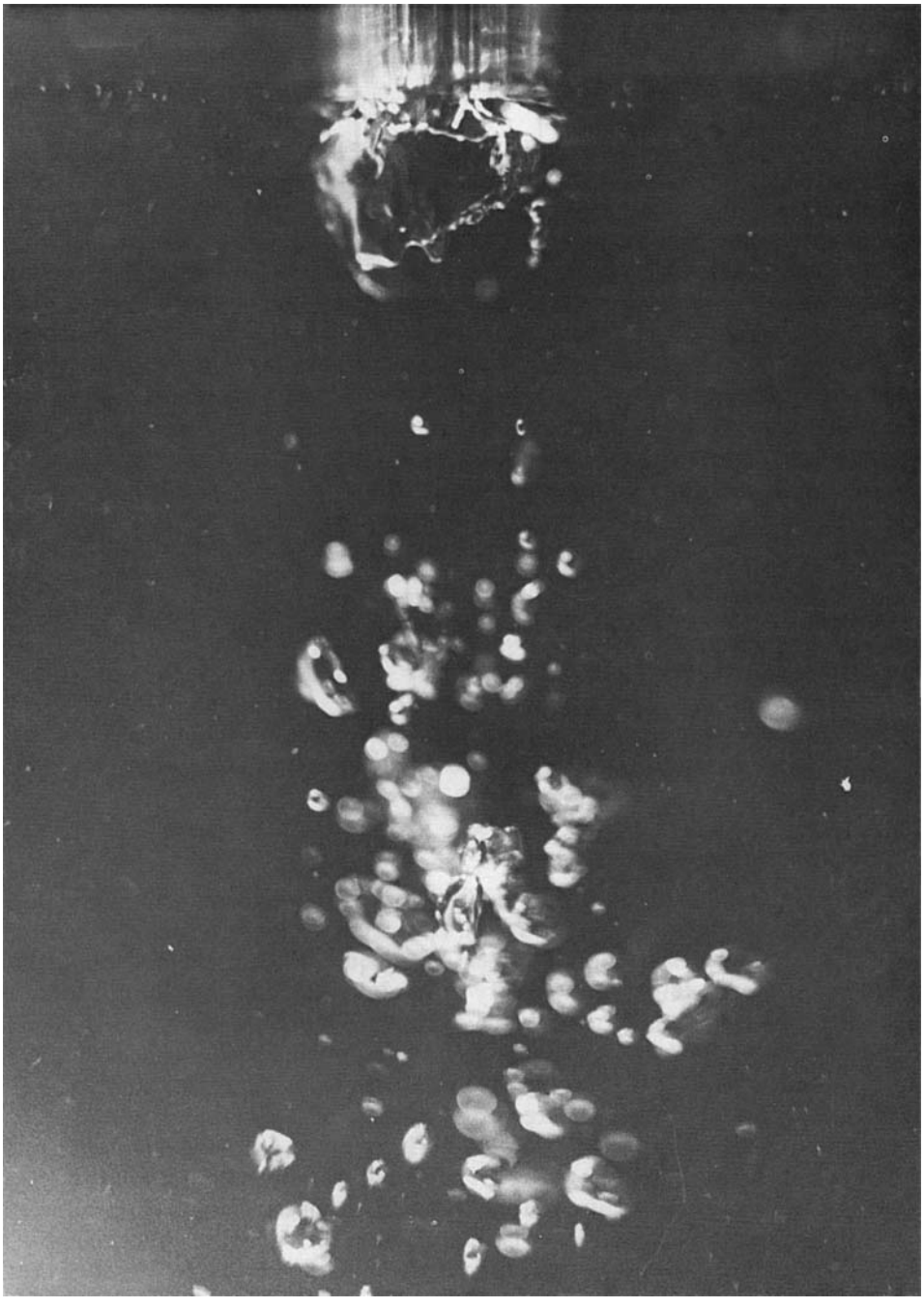

FIGURE 1. Water jet falling into a pool of water at rest. The camera looks at the free surface slightly from below. A short film of air envelops the jet around its entry point into the receiving liquid, clearly visible at the top of the figure. The diameter of the jet is slightly less than 1 cm and its velocity about 0.7 m/s. (Courtesy of Professor J. Duncan.)

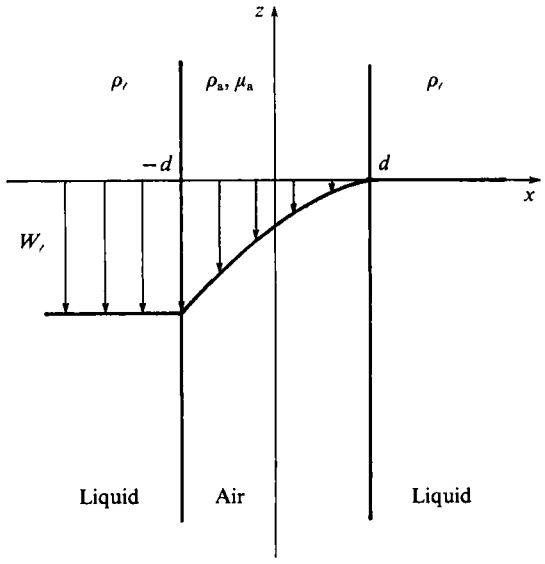

FIGURE 2. Flow configuration assumed for the air film model. A plane film of thickness $2d$ separates two half-spaces occupied by a liquid. The liquid to the left of the film is in uniform downward motion with velocity W_ℓ. On the other side the liquid is at rest. Gravity is directed downward. The viscosity of the liquid is neglected.

and nonlinear effects are not included. In spite of these shortcomings, the following analysis appears to be a necessary step towards an understanding of the process.

2. The unperturbed state

The unperturbed state we consider consists of a thin, plane air film separating two half-spaces occupied by a liquid (figure 2). Gravity is acting downward in a direction parallel to the undisturbed film surfaces. The liquid to the left of the film has an undisturbed uniform downward velocity of modulus W_ℓ, while the liquid to its right is quiescent in the unperturbed state. This stipulation defines our frame of reference, which is appropriate for the case of a large-diameter jet plunging in a liquid or of skirt formation around a large-diameter bubble. In these examples curvature effects due to axial symmetry can be disregarded in view of the thinness of the film. The parameter expressing the acceleration of gravity may be adjusted to incorporate the effect of pressure gradients of a different origin in the direction parallel to the film.

Since the air film is very thin and its Reynolds number relatively small, we take the air to be an incompressible, viscous fluid. The viscosity of the liquid will, however, be ignored. This approximation is rendered necessary by the fact that the system is taken of infinite extent in the vertical direction and with no boundaries in the horizontal one. As far as the liquid is concerned, the effect of this viscous boundary layer is to distort the velocity distribution from the uniform value W_ℓ, which is assumed in the model, to a non-uniform one. If W_i is the vertical velocity at the interface, we can estimate its deviation from W_ℓ by balancing the tangential stresses at the interface,

$$\mu_\ell \frac{W_\ell - W_i}{\delta_\ell} \sim \mu_a \frac{W_i}{2d}, \tag{1}$$

where μ_ℓ and μ_a denote the liquid and air viscosities, $2d$ is the thickness of the air film, and δ_ℓ is the thickness of the viscous boundary layer in the liquid. From this relation we find

$$\frac{W_i}{W_\ell} \sim \left(1+\frac{\mu_a}{\mu_\ell}\frac{\delta_\ell}{2d}\right)^{-1} \sim 1-\frac{\mu_a}{\mu_\ell}\frac{\delta_\ell}{2d}. \tag{2}$$

If we use the estimate $\delta_\ell \sim (z\nu_\ell/W_\ell)^{\frac{1}{2}}$ for the thickness of the viscous boundary layer at a depth z in a liquid with kinematic viscosity ν_ℓ, we find, for a 1 m/s water jet at a depth of 1 cm below the free surface, $\delta_\ell \approx 100\ \mu$m, which is comparable with the thickness of the air film. Since $\mu_a \ll \mu_\ell$, the viscous correction to the liquid velocity profile is thus seen to be very small and therefore the consequences of our approximation should be minor. Further comments on this point will be given in the last section.

The neglect of the liquid viscosity forces us to drop some of the interface conditions. Continuity of normal stresses and velocities across the interface can be imposed on both the liquid and gas sides. No other conditions can be imposed on the liquid side, while on the gas side we can in principle use continuity of tangential velocity or of tangential stresses. The previous argument shows that the latter alternative would be incompatible with the neglect of viscous effects in the liquid, and therefore we shall impose continuity of the tangential velocity. These boundary conditions are used on both the unperturbed and the perturbed states.

It is readily verified that the velocity distribution

$$\boldsymbol{U}(x) = W(x)\,\boldsymbol{e}_3 = \left[-\frac{\rho_\ell-\rho_a}{2\mu_a}g(x^2-d^2)+W_\ell\frac{x-d}{2d}\right]\boldsymbol{e}_3, \tag{3}$$

for the air flow in the film satisfies the conditions $W(-d) = -W_\ell$, $W(d) = 0$. Here $\boldsymbol{e}_3$ is the unit vector in the direction of the z-axis, which is taken vertically upward. The x-axis points toward the body of liquid at rest, with the origin in the centre of the film (figure 2). Furthermore, ρ_ℓ and ρ_a denote the liquid and the air densities and g is the acceleration due to gravity. The pressure distribution in the film is given by

$$P = P_0-\rho_\ell g z, \tag{4}$$

where P_0 is the pressure at $z = 0$. The pressure gradient in the gas given by this equation is constant and is therefore able to balance the hydrostatic pressure in the liquid. The base flow (3) is given by the superposition of a Poiseuille component, which is sustained by the pressure gradient due to gravity, and of a Couette component, which satisfies continuity of velocity at the air–liquid interfaces. The total transport of air in the film is

$$\dot{V} = \int_{-d}^{d} W(x)\,\mathrm{d}x = \left(\frac{2}{3}\frac{\rho_\ell-\rho_a}{\mu_a}gd^2-W_\ell\right)d. \tag{5}$$

This model for the unperturbed state has been used by Guthrie & Bradshaw (1969) in their study of bubble skirts.

The film thickness appears as a free parameter in this base state. In the stability analysis that follows, we shall present results for different values of this quantity. However, it may be noted that two special values exist, one corresponding to no stress being exerted on the right-hand liquid surface, and one corresponding to no mass being transported in the film. These two values are $d = d_1 = [\mu_a W_\ell/2(\rho_\ell-\rho_a)g]^{\frac{1}{2}}$ and $d = d_2 = \sqrt{3}d_1$ respectively. When $d < d_1$ the air flows downward only. When

$d_1 < d < d_2$, a region of upward flow is also present, but the net volume flow is still downward. Finally, for $d_2 < d$, there is a net volume flow upward, a situation of no interest for the study of air entrainment. For water and air at 20 °C, $\mu_a = 1.81 \times 10^{-4}$ g cm^{-1} s^{-1}, $\rho_a = 1.205 \times 10^{-3}$ g cm^{-3}, $\rho_\ell = 0.998$ g cm^{-3}, and, with $W_\ell = 100$ cm s^{-1}, we find for d_1 and d_2 the values 30.4 μm and 52.5 μm, respectively. This order of magnitude is in good agreement with the measurements of Guthrie & Bradshaw (1969).

3. Linear stability analysis: governing equations

It is convenient to pass to dimensionless quantities and for this purpose we choose d, W_ℓ, $\rho_a d^2/\mu_a$, and $\mu_a W_\ell/d$, as characteristic length, velocity, time and pressure, respectively. The choice of the last two scales is dictated by the importance of viscosity for the dynamics of the film; indeed, the Reynolds number of the air flow,

$$Re = \frac{\rho_a W_\ell d}{\mu_a}, \tag{6}$$

has values of order one (e.g. for $W_\ell = 1$ m s^{-1} and $d = 30$ μm, $Re = 1.99$). The base velocity profile rewritten in dimensionless form is

$$W = -\alpha(x^2-1) + \tfrac{1}{2}(x-1), \tag{7}$$

where the parameter α, which may be regarded as a measure of the relative importance of the Poiseuille to the Couette components of the base flow, is given by

$$\alpha = \frac{\rho_\ell - \rho_a}{2\mu_a W_\ell} g d^2. \tag{8}$$

The special values $\alpha = \frac{1}{4}$ and $\alpha = \frac{3}{4}$ correspond to zero stress at the right-hand interface and to zero net mass transport in the film, respectively. Two other non-dimensional parameters enter the problem: the density ratio

$$\epsilon = \frac{\rho_a}{\rho_\ell}, \tag{9}$$

which equals 1.207×10^{-3} for air–water at 20 °C; and the capillary number

$$Ca = \frac{\mu_a W_\ell}{\sigma}. \tag{10}$$

This quantity is a measure of the ratio of viscous to capillary effects. Typical values are of the order of 10^{-3}. For example, again for water–air at 20 °C, with $W_\ell = 1$ m/s, $Ca \approx 2.5 \times 10^{-4}$. From now on all quantities will be dimensionless, but no special notation will be used.

Recently Hesla, Pranckh & Preziosi (1986) have extended Squire's theorem on the stability of parallel flows to the case of more than one layer of immiscible fluids. This result would be directly applicable to the problem investigated here only if the viscosity of the liquid had been retained. However, insofar as the present model is intended as an approximation to the fully viscous situation, we feel justified in considering only two-dimensional disturbances.

Indices ℓ and r will be used to denote the regions occupied by the liquid to the left and to the right of the air film, $x < -1$ and $x > 1$, respectively. The perturbed interfaces are described by the equations

$$S_{\ell,\mathrm{r}}(x,z,t) = x - [\mp 1 + \eta_{\ell,\mathrm{r}}(z,t)] \equiv 0. \tag{11}$$

The continuity equation,

$$\nabla \cdot \boldsymbol{u}_{\ell,\mathrm{r}} = 0, \tag{12}$$

and the momentum equations,

$$\frac{\partial \boldsymbol{u}_\ell}{\partial t} - Re\frac{\partial \boldsymbol{u}_\ell}{\partial z} = -\epsilon \nabla p_\ell, \tag{13}$$

$$\frac{\partial \boldsymbol{u}_\mathrm{r}}{\partial t} = -\epsilon \nabla p_\mathrm{r}, \tag{14}$$

are the linearized disturbance equations in the liquid. In the air, we have the continuity equation $\nabla \cdot \boldsymbol{u} = 0$ and the momentum equation,

$$\frac{\partial \boldsymbol{u}}{\partial t} + Re\left(W\frac{\partial \boldsymbol{u}}{\partial z} + u\frac{\mathrm{d}W}{\mathrm{d}x}\boldsymbol{e}_3\right) = -\nabla p + \nabla^2 \boldsymbol{u}. \tag{15}$$

By imposing continuity of velocities at the air–liquid interfaces it follows that

$$u_{\ell,\mathrm{r}}(\mp 1, z, t) = u(\mp 1, z, t), \tag{16}$$

$$w_{\ell,\mathrm{r}}(\mp 1, z, t) = w(\mp 1, z, t) + \frac{\mathrm{d}W}{\mathrm{d}x}(\mp 1)\,\eta_{\ell,\mathrm{r}}(z,t). \tag{17}$$

From the continuity of normal stresses we obtain

$$p_{\ell,\mathrm{r}}(\mp 1, z, t) - p(\mp 1, z, t) = -2\left[\frac{\partial u}{\partial x}(\mp 1, z, t) - \frac{\mathrm{d}W}{\mathrm{d}x}(\mp 1)\frac{\partial \eta_{\ell,\mathrm{r}}}{\partial z}(z,t)\right] \mp Ca^{-1}\frac{\partial^2 \eta_{\ell,\mathrm{r}}}{\partial z^2}(z,t), \tag{18}$$

and from the kinematic conditions

$$\frac{\partial \eta_\ell}{\partial t}(z,t) = Re\left[u(-1,z,t) + \frac{\partial \eta_\ell}{\partial z}(z,t)\right], \tag{19}$$

$$\frac{\partial \eta_\mathrm{r}}{\partial t}(z,t) = Re\, u(1,z,t). \tag{20}$$

Finally, as $|x|$ tends to infinity, we require the disturbances to vanish.

Since the problem is clearly linear and homogeneous and the differential equations have coefficients independent of z and t we can look for solutions of the form

$$\boldsymbol{u}(x,z,t) = \hat{\boldsymbol{u}}(x)\,\mathrm{e}^{st+\mathrm{i}kz}, \tag{21}$$

and similarly for w, p and $\eta_{\ell,\mathrm{r}}$. The introduction of the normal modes allows us to solve the problem in the two regions occupied by the liquid in terms of film quantities. Simple manipulations lead to the following equations for $\hat{u}_{\ell,\mathrm{r}}$:

$$\hat{u}''_{\ell,\mathrm{r}} - k^2\hat{u}_{\ell,\mathrm{r}} = 0, \tag{22}$$

where the prime denotes differentiation with respect to x. By imposing that the amplitudes vanish at infinity, we find

$$\hat{u}_{\ell,\mathrm{r}} = A_{\ell,\mathrm{r}}\,\mathrm{e}^{\pm kx}, \quad \hat{w}_{\ell,\mathrm{r}} = \pm \mathrm{i}\hat{u}_{\ell,\mathrm{r}}, \tag{23}$$

for the velocity fields and

$$\hat{p}_\ell = -\frac{s - \mathrm{i}\,Re\,k}{\epsilon k}\hat{u}_\ell, \quad \hat{p}_\mathrm{r} = \frac{s}{\epsilon k}\hat{u}_\mathrm{r}, \tag{24}$$

for the pressure fields. The integration constants $A_{\ell,\mathrm{r}}$ are to be determined by matching the velocity profiles in the liquid and in the air.

It is now possible to derive a closed system of equations and boundary conditions for the amplitudes of the normal modes in the air film. Upon introduction of the normal modes in the continuity and momentum equations one obtains

$$\hat{u}' + \mathrm{i}k\hat{w} = 0, \tag{25}$$

$$\hat{u}'' - (s + \mathrm{i}W\,Re\,k + k^2)\,\hat{u} = \hat{p}', \tag{26}$$

$$\hat{w}'' - (s + \mathrm{i}W\,Re\,k + k^2)\,\hat{w} - Re\,W'\,\hat{u} = \mathrm{i}k\hat{p}. \tag{27}$$

The boundary conditions (16) become

$$\hat{u}_{\ell,\mathrm{r}}(\mp 1) = \hat{u}(\mp 1). \tag{28}$$

Together with (23) and (24), these enable us to rewrite (17)–(20) as

$$\hat{w}(\mp 1) = \pm \mathrm{i}\hat{u}(\mp 1) - W'(\mp 1)\,\hat{\eta}_{\ell,\mathrm{r}}, \tag{29}$$

$$\hat{p}(-1) = -\frac{\tilde{s}}{\epsilon k}\hat{u}(-1) + 2[\hat{u}'(-1) - \mathrm{i}W'(-1)\,k\hat{\eta}_\ell] - Ca^{-1}k^2\,\hat{\eta}_\ell, \tag{30}$$

$$\hat{p}(1) = \frac{s}{\epsilon k}\hat{u}(1) + 2[\hat{u}'(1) - \mathrm{i}W'(1)\,k\hat{\eta}_\mathrm{r}] + Ca^{-1}k^2\,\hat{\eta}_\mathrm{r}, \tag{31}$$

$$Re\,\hat{u}(-1) = \tilde{s}\hat{\eta}_\ell, \tag{32}$$

$$Re\,\hat{u}(1) = s\hat{\eta}_\mathrm{r}, \tag{33}$$

where we have defined

$$\tilde{s} = s - \mathrm{i}\,Re\,k. \tag{34}$$

The same problem can also be phrased in terms of ψ, the stream function of the disturbance velocity, which leads to a form useful for numerical work. If we let

$$\psi(x, z, t) = \hat{\psi}(x)\,\mathrm{e}^{st + \mathrm{i}kz}, \tag{35}$$

then

$$\hat{u} = \mathrm{i}k\hat{\psi}, \quad \hat{w} = -\hat{\psi}', \tag{36}$$

and (27) gives

$$\hat{p} = \frac{\mathrm{i}}{k}[\hat{\psi}''' - (s + \mathrm{i}W\,Re\,k + k^2)\,\hat{\psi}' + \mathrm{i}W'\,Re\,k\hat{\psi}]. \tag{37}$$

Upon substitution of (35) and (36) into (26), we obtain the Orr–Sommerfeld equation

$$\hat{\psi}'''' - (s + \mathrm{i}W\,Re\,k + 2k^2)\,\hat{\psi}'' + [\mathrm{i}W''\,Re\,k + (s + \mathrm{i}W\,Re\,k + k^2)\,k^2]\,\hat{\psi} = 0. \tag{38}$$

The appropriate boundary conditions are obtained from (29)–(31), by using (32) and (33), and are

$$\tilde{s}\hat{\psi}'(-1) = k[\tilde{s} + \mathrm{i}W'(-1)Re]\,\hat{\psi}(-1), \tag{39}$$

$$s\hat{\psi}'(1) = -k[s - \mathrm{i}W'(1)Re]\,\hat{\psi}(1), \tag{40}$$

$$\tilde{s}\hat{\psi}'''(-1) = k\{(1-\epsilon^{-1})\,\tilde{s}^2 + 3k^2\tilde{s} - [Ca^{-1}k - \mathrm{i}W'(-1)]Re\,k^2\}\,\hat{\psi}(-1), \tag{41}$$

$$s\hat{\psi}'''(1) = -k\{(1-\epsilon^{-1})\,s^2 + 3k^2 s - [Ca^{-1}k + \mathrm{i}W'(1)]Re\,k^2\}\,\hat{\psi}(1). \tag{42}$$

Once the problem for $\hat{\psi}$ has been solved, the amplitude of the surface displacements can be calculated from (32) and (33) which, in terms of $\hat{\psi}$, are

$$\tilde{s}\hat{\eta}_\ell = \mathrm{i}Re\,k\hat{\psi}(-1), \quad s\hat{\eta}_\mathrm{r} = \mathrm{i}Re\,k\hat{\psi}(1). \tag{43}$$

4. Long-wave asymptotics

The perturbation problem formulated in the previous section cannot be solved analytically in closed form. Before carrying out a numerical integration, it is useful to study the asymptotic behaviour of the dispersion relation $s = s(k)$ in the limits of wavelengths large and small compared with the thickness of the air film. These results enable us to identify and classify the eigenvalues of the system and to gain some insight into the physical mechanisms of the instability. Moreover, the approximate results for long wavelengths have been used as initial guesses for the iterative process upon which the numerical method of solution is based. Here we discuss the long-wavelength limit. The next section is devoted to the analysis of the short-wavelength case.

The details of the asymptotic analysis for $k \to 0$ are rather straightforward and can be found in the Appendix. Here we describe some results and note that the calculations are considerably simplified by dealing with (25)–(27) directly, rather than by using the stream-function formulation. If the latter course were taken, the determination of s to the leading order would require the solution of the problem for $\hat{\psi}$ to the second order.

Upon writing

$$s(k) = s_0 + s_1 k + s_2 k^2 + \ldots, \tag{44}$$

we find in the Appendix that s_0 can either vanish or take the infinity of values

$$s_0^{(n)} = -\tfrac{1}{4}n^2\pi^2, \quad n = 1, 2, \ldots. \tag{45}$$

These higher modes are heavily damped and are not expected to lead to an unstable behaviour. They will be briefly considered later. For the present purposes the most interesting modes are those for which s_0 vanishes. To study this case in more detail we let

$$s = k(s_0 + ks_1 + \ldots), \tag{46}$$

and find three different solutions,

$$s^{(\pm)} = \frac{1}{2}\left[\mathrm{i} \pm \left(1 - 8\mathrm{i}\frac{\alpha\epsilon}{Re}\right)^{\frac{1}{2}}\right] Re\,k + O(k^2), \tag{47}$$

$$s^{(0)} = \mathrm{i}(\tfrac{1}{2} - 2\alpha)\,Re\,k + (1 - 16\alpha^2)\left[\frac{Re}{30} + \frac{\epsilon + \mathrm{i}2\alpha\,Re}{(1+16\alpha^2)\,Re - \mathrm{i}8\alpha\epsilon}\right] Re\,k^2 + O(k^3). \tag{48}$$

The mode $s^{(+)}$ is evidently unstable and it is easy to see that it is associated to an

instability of the Kelvin–Helmholtz type, as expected. Indeed, the standard result for the growth rate of this instability (Lamb 1932; Chandrasekhar 1961) is, in our dimensionless units,

$$s_{\mathrm{KH}}^{(\pm)} = \frac{1}{2}\left[\mathrm{i} \pm \left(1 - 4\frac{\epsilon}{Re\,Ca}k\right)^{\frac{1}{2}}\right] Re\,k, \tag{49}$$

and therefore, to leading order in k, coincides with (47) up to the small correction $8\alpha\epsilon/Re$ which is due to the effect of the buoyancy of the film. This interpretation is strengthened by the fact that the displacements of the left- and right-hand interfaces are equal, to the leading order in k, so that the air film behaves approximately as a single surface of discontinuity, although with a complicated internal structure. Note that, in (49), the surface tension contribution of the standard Kelvin–Helmholtz result has been multiplied by two to properly account for the two interfaces bounding the air film.

If, in the study of the stability characteristics of a parallel shear flow, a rigid boundary is replaced with a free surface or an interface, two new surface modes appear in addition to the shear modes that were present in the original flow. In general the surface modes are waves travelling in opposite directions and they are less stable than the shear modes. In the configuration that we are considering here there are two interfaces, and hence four surface modes. As will be clearer from a consideration of the short-wavelength limit, two of them are $s^{(\pm)}$ while the other two are $s^{(0)}$ and $s^{(1)}$. It may be noted that a mode similar to the root $s^{(0)}$ is found in the study of the stability of a film flowing down an inclined plane (Benjamin 1957; Yih 1963; Smith 1990). In that case, as in the present one, the real part of the eigenvalue is of order k^2, and can be positive or negative depending on the inclination of the plane and the Reynolds number. Here the sign of the real part of $s^{(0)}$ depends on the parameter α, being positive for $\alpha > \frac{1}{4}$. An eigenvalue similar to $s^{(1)}$ is also found in the problem studied by Yih (1963), after the correction of what appears to be an algebraic error.† It may be concluded that the modes corresponding to $s^{(0)}$ and $s^{(1)}$ are characteristic of the stability of parallel flows with free boundaries.

The modes (45) with n greater than 1 are shear modes, closely related to those in the spectrum of parallel flows between solid boundaries. We refer to Birikh, Gershuni & Zhukhovitskii (1966) for a study of the eigenvalues and the eigenfunctions of such flows in the long-wavelength limit at low Reynolds numbers. To the leading order in k, perturbations for which the stream function is alternatively even and odd are found. The eigenvalues associated with the even eigenfunctions are given by (45) with $n = 2, 4, 6, \ldots$. They coincide with those of our system because to this order in k the free-surface displacements vanish when n is even (see the Appendix). The eigenvalues associated with the odd eigenfunctions are determined by

$$(-S)^{\frac{1}{2}}\cot(-S)^{\frac{1}{2}} = 1. \tag{50}$$

The first few solutions of this equation are $S^{(1)} = -20.191$, $S^{(3)} = -59.680$, $S^{(5)} = -118.90\ldots$. They are somewhat smaller in modulus than the corresponding eigenvalues of our system, $s_0^{(3)} = -22.207$, $s_0^{(5)} = -61.685$, $s_0^{(7)} = -120.90\ldots$, but the

† In section VIII, where he compares the spectrum of a plane Poiseuille flow with the one of a flow down an inclined plane, he considers the long-wave limit for the free-surface flow. Imposing the boundary condition $\beta^2\phi'(0) - \phi'''(0) = 0$ on $\phi = A + By + Ce^{\beta y} + De^{-\beta y}$, he erroneously deduces $B = -4\beta D$ instead of $B = 0$. The correct eigencondition is $\cosh\beta = 0$, the roots of which are $\beta^2 = -\frac{1}{4}(n\pi)^2$, $n = 1, 3, 5, \ldots$. Since β^2 is the growth rate, the first of these eigenvalues coincides with $s_0^{(1)}$.

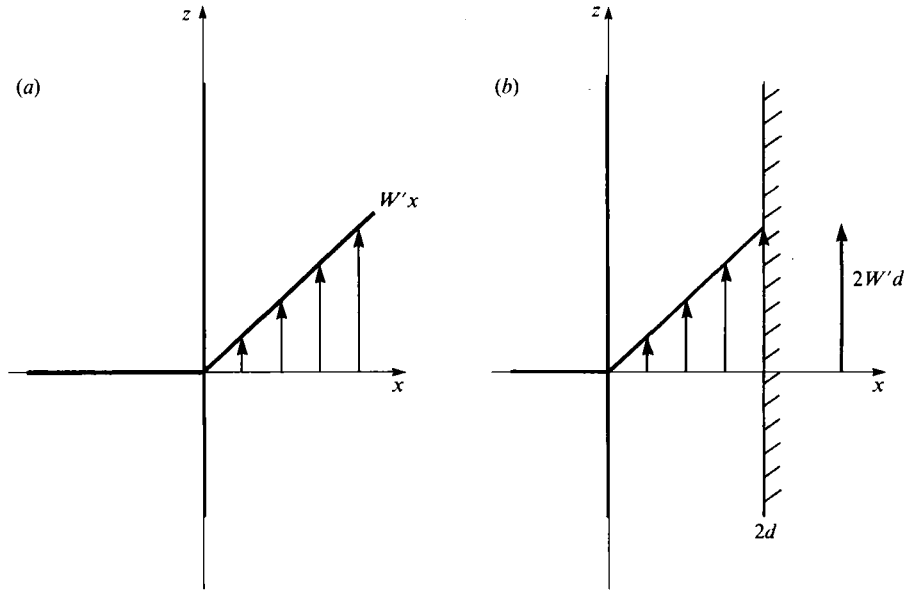

FIGURE 3. Flow configurations for the viscous instability model. The left half-space is occupied by an inviscid liquid at rest. The viscous fluid to the right of the interface is in linear shearing motion with shear rate W'. (*a*) Unbounded case; (*b*) bounded case: a vertical wall is placed at a distance $2d$ from the interface.

difference $S^{(n-2)} - s_0^{(n)}$ tends to zero as $n \to \infty$. This difference may be explained by observing that, as shown in the Appendix, when n is odd the displacements of the two interfaces are opposite. This circumstance causes a longitudinal flow in the film with a viscous dissipation larger than in the case of rigid boundaries. Since the interface displacement is proportional to n^{-3} while the velocity disturbance is proportional to n^{-1}, as n increases, this difference tends to disappear and (50) becomes a closer and closer approximation to the eigenvalues of the present problem.

5. Viscous instability

At wavelengths very short compared with the film thickness, one expects the disturbances to affect only a thin region around each interface. In this wavelength range the two interfaces should become essentially uncoupled and each one of them should behave very similarly to the interface of a model configuration in which a single free surface separates a viscous from an inviscid fluid. The spectrum of the complete problem is therefore expected to reduce to the combination of two such spectra. These considerations lead us to the study of the stability of a two-dimensional shear flow with an interface across which viscosity is discontinuous. Since the results of the treatment of this problem given by Hooper & Boyd (1983) cannot be readily adapted to the case of present concern in which one of the two fluids is inviscid, we develop here the analysis *ab initio*.

Consider a half-space occupied by an inviscid fluid of density ρ_ℓ, moving with uniform velocity $\boldsymbol{U}_\ell = W_0 \boldsymbol{e}_3$. The other half-space contains a second fluid of density ρ_a and viscosity μ_a. Its unperturbed velocity distribution is $\boldsymbol{U}_a = (W_0 + W'x)\boldsymbol{e}_3$ (figure 3*a*). Since the condition of continuity of the tangential stresses cannot be imposed at a viscous–inviscid interface, here the shear rate W' is an independent parameter of

the problem. It is in this feature that the present situation differs from that studied by Hooper & Boyd, for which the shear rate was dictated by the continuity of tangential stresses.

In addition to the previous configuration, we shall also study the case in which the viscous fluid has a finite thickness $2d$ and is bounded by a rigid wall. In order to maintain the linear velocity distribution in the film, the wall has an upward (dimensional) velocity given by $W_0+2W'd$ (figure 3*b*). In this analysis, we have been motivated by the following considerations. If the wavelength is very large, since the air film is taken to be incompressible, both interfaces must undergo non-zero displacements. At moderate or short wavelengths, however, in view of the very large density difference between the two fluids, one expects the high inertia of the liquid to strongly limit the participation of one interface to a perturbation mode corresponding to the other one. Thus, the substitution of the 'passive' interface with a solid boundary should change but little the system's response. Indeed, it will be seen that endowing the viscous fluid with a finite extent greatly extends the degree to which this simpler model simulates the complete problem of concern in the present paper.

It is readily shown that the only effect of the velocity W_0 is to add the purely imaginary term $\mathrm{i}W_0 k$ to the eigenvalues. We shall therefore assume $W_0 = 0$ in the following, which is equivalent to performing a Galilean transformation. Furthermore, on the basis of symmetry considerations, one expects the real part of the growth rate s not to depend on the sign of W'. Indeed, it can be proven that the complex conjugate of any eigenvalue corresponding to a shear rate W' is an eigenvalue of the reversed-flow configuration with the shear rate $-W'$. This fact permits us to consider only positive values of W'.

Intrinsic scales for the model problem are the lengthscale $(\mu_a/\rho_a W')^{\frac{1}{2}}$, the velocity scale $(\mu_a W'/\rho_a)^{\frac{1}{2}}$ and the timescale W'^{-1}. In addition, for the bounded configuration, there are a characteristic length d, velocity $W'd$, and time $\rho_a d^2/\mu_a$. The former set of units is the most natural one. The dimensionless formulation of the unbounded problem that follows from this choice depends only on one parameter related to the surface tension, whereas the bounded problem depends also on the dimensionless distance of the wall from the interface. When this distance tends to infinity, one recovers the unbounded case as a limit of the bounded one. The study of the stability characteristics of the interface as a function of the surface tension and distance of the wall for a fixed shear rate at the interface is, thus, quite straightforward. In order to explain the stability characteristics of the air film, however, we are more interested in the dependence of the growth rate on the interfacial shear rate for a given surface tension and a given thickness of the region occupied by the viscous fluid. In view of this objective, it is more convenient to use the second set of units. It is then found that both the finite and infinite problems are governed by two parameters, a Reynolds number

$$Re_v = \frac{\rho_a W' d^2}{\mu_a},$$

which may be interpreted as a measure of the magnitude of the shear rate, and the parameter

$$\Gamma_v = \rho_a \frac{\sigma d}{\mu_a^2},$$

which is the ratio of the Reynolds number Re_v to the capillary number $Ca_v =$

$\mu_a W' d/\sigma$. Dimensionless quantities will be used henceforth, although no special notation will be used.

As for the original problem, we introduce a stream function ψ to describe the flow in the viscous fluid. The complex amplitude $\hat{\psi}$ of any normal mode satisfies the Orr–Sommerfeld equation which, upon scaling and substitution of the unperturbed velocity profile, may be written as

$$\left(\frac{\mathrm{d}^2}{\mathrm{d}x^2}-k^2\right)\left[\left(\frac{\mathrm{d}^2}{\mathrm{d}x^2}-k^2\right)\hat{\psi}-(s+\mathrm{i}Re_{\mathrm{v}}kx)\hat{\psi}\right]=0. \tag{51}$$

At the interface the same boundary conditions as at the left surface of the film apply. Making the change of variable $x \to x+1$, from (39) and (41) we obtain

$$s\hat{\psi}'(0) = k[s+\mathrm{i}Re_{\mathrm{v}}]\hat{\psi}(0), \tag{52}$$

$$s\hat{\psi}'''(0) = k[(1-\epsilon^{-1})s^2+3k^2s+\mathrm{i}Re_{\mathrm{v}}k^2-\Gamma_{\mathrm{v}}k^3]\hat{\psi}(0). \tag{53}$$

The other two boundary conditions (40) and (42) are replaced by imposing that the disturbances tend to zero as x tends to ∞ in the unbounded case, whereas in the finite case the disturbance velocity must vanish at the wall, that is

$$\hat{\psi}(2) = 0, \tag{54}$$

$$\hat{\psi}'(2) = 0. \tag{55}$$

The derivation of the eigencondition follows the same steps as in the cases treated by Hooper & Boyd; however, the algebra is much simpler. The solutions of (51) are expressed in terms of the Airy functions of complex arguments

$$A_j(x) = \mathrm{Ai}\left(\frac{Re_{\mathrm{v}}kx-\mathrm{i}(s+k^2)}{(Re_{\mathrm{v}}k)^{\frac{2}{3}}}\mathrm{e}^{\mathrm{i}\theta_j}\right), \quad j=1,2, \tag{56}$$

where $\theta_1 = \frac{1}{6}\pi$ and $\theta_2 = \frac{5}{6}\pi$. In the unbounded case the disturbances vanish at infinity. This condition restricts the set of acceptable solutions to the form

$$\hat{\psi}(x) = c_1\,\mathrm{e}^{-kx}-\frac{c_2}{2k}\left\{\mathrm{e}^{-kx}\int_0^x \mathrm{e}^{ky}A_1(y)\,\mathrm{d}y+\mathrm{e}^{kx}\int_x^\infty \mathrm{e}^{-ky}A_1(y)\,\mathrm{d}y\right\}, \tag{57}$$

where c_1 and c_2 are integration constants. By imposing the boundary conditions (52) and (53), the following linear system of equations in c_1, c_2 is obtained:

$$4k^2sc_1+\mathrm{i}Re_{\mathrm{v}}(2k^2c_1-Jc_2) = 0,$$

$$[(1-\epsilon^{-1})s^2+4k^2s+\mathrm{i}Re_{\mathrm{v}}k^2-\Gamma_{\mathrm{v}}k^3]\,(2k^2c_1-Jc_2)-2kA_1'(0)sc_2 = 0.$$

For the system to possess non-trivial solutions the determinant must vanish, which leads to the dispersion relation

$$[(1-\epsilon^{-1})s^2+2k^2s-\Gamma_{\mathrm{v}}k^3]J+(2s+\mathrm{i}Re_{\mathrm{v}})kA_1'(0) = 0, \tag{58}$$

where

$$J = k\int_0^\infty \mathrm{e}^{-ky}A_1(y)\,\mathrm{d}y. \tag{59}$$

For the bounded configuration, we impose conditions (54) and (55) on the general solution of (51), obtaining

$$\hat{\psi}(x) = c_3\int_x^2 \sinh[k(y-x)]A_1(y)\,\mathrm{d}y+c_4\int_x^2 \sinh[k(y-x)]A_2(y)\,\mathrm{d}y, \tag{60}$$

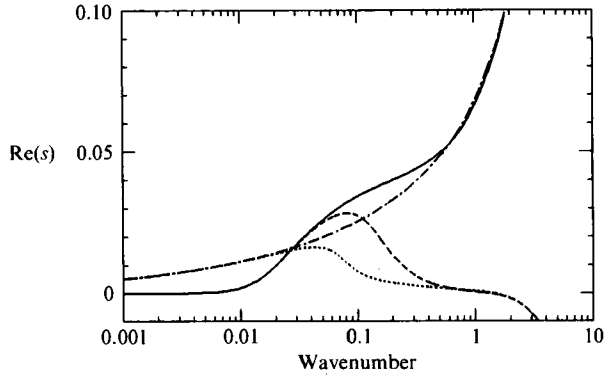

FIGURE 4. Effect of surface tension on the viscous instability. Dimensionless growth rate Re(s) *vs.* the dimensionless wavenumber k for $Re_v = 2$. No surface tension, $\Gamma_v = 0$: ——, bounded configuration; ·–·–·, unbounded configuration. $\Gamma_v = 1000$: – – –, bounded configuration; · · · · ·, unbounded configuration.

where c_3 and c_4 are integration constants. Upon substitution into the interface conditions (52) and (53), we find a linear system in these quantities:

$$(s+\mathrm{i}Re_v)(J_{S1}c_3+J_{S2}c_4)+s(J_{C1}c_3+J_{C2}c_4)=0,$$

$$[(1-\epsilon^{-1})s^2+3k^2s+\mathrm{i}Re_v k^2-\Gamma_v k^3](J_{S1}c_3+J_{S2}c_4)$$
$$+k^2s(J_{C1}c_3+J_{C2}c_4)-s[A_1'(0)c_3+A_2'(0)c_4]=0,$$

where

$$J_{Sj}=\int_0^2 \sinh(ky)A_j(y)\,\mathrm{d}y, \tag{61}$$

$$J_{Cj}=\int_0^2 \cosh(ky)A_j(y)\,\mathrm{d}y, \tag{62}$$

with $j = 1, 2$. This system has non-trivial solutions if and only if

$$[(1-\epsilon^{-1})s^2+2k^2s-\Gamma_v k^3](J_{S2}J_{C1}-J_{S1}J_{C2})$$
$$+s[A_1'(0)(J_{S2}+J_{C2})-A_2'(0)(J_{S1}+J_{C1})]+\mathrm{i}Re_v[A_1'(0)J_{S2}-A_2'(0)J_{S1}]=0, \tag{63}$$

which is the dispersion relation for the bounded case.

For the purpose of shedding light on the stability of the air film we are interested only in the first modes of these model problems, which are associated with the motion of the free surface. To obtain the results which follow, the dispersion relations have been solved numerically by means of the Newton–Raphson proccdure. For the evaluation of the Airy functions and their derivatives, use has been made of the algorithm developed by Schulten, Anderson & Gordon (1979).

Figure 4 shows the growth rate Re (s) of the unstable mode versus the wavenumber for the cases $\epsilon = 1.207 \times 10^{-3}$, $Re_v = 2$, $\Gamma_v = 0$ and 1000 both for the bounded and unbounded configurations. When surface tension is neglected ($\Gamma_v = 0$, continuous and dash-and-dot lines), the interface is unstable for all wavelengths, with the growth rate a monotonic increasing function of the wavenumber. The rigid boundary (continuous line) has a substantial stabilizing effect on long-wavelength disturbances, but acts as a destabilizing factor in the region $0.01 < k < 1$, approximately. This fact will be seen in the next section to play a major role in the air film instability studied in the present paper. The dashed and the dotted lines are for $\Gamma_v = 1000$, for bounded

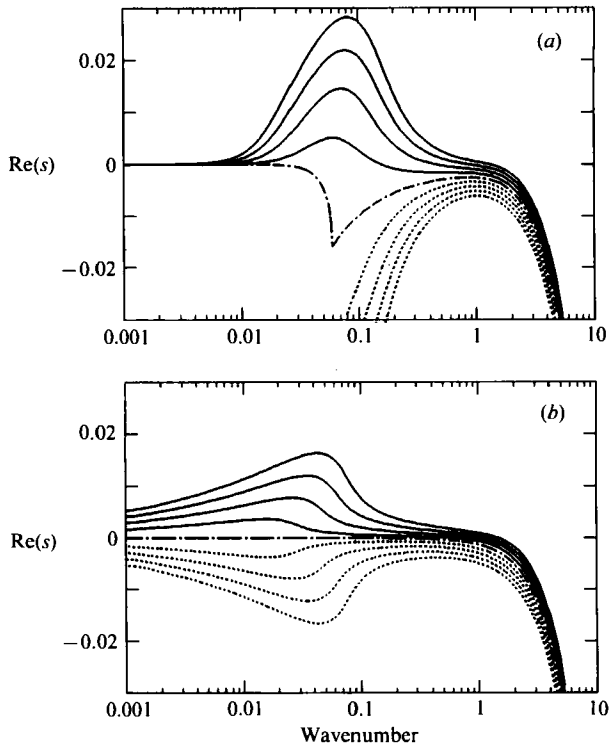

FIGURE 5. Dimensionless growth rate Re(s) *vs.* the dimensionless wavenumber k for the two surface modes of the viscous instability for $\Gamma_v = 1000$, $Re_v = 0, 0.5, 1.0, 1.5, 2.0$. (*a*) Bounded configuration; (*b*) unbounded configuration. ——, Unstable modes; · · · · ·, stable modes. For $Re_v = 0$ (·–·–·) the real parts of the two modes coincide. Unstable modes become more unstable with increasing Re_v, and conversely for the stable modes.

and unbounded regions, respectively. As expected, surface tension stabilizes short wavelengths. Of greater significance, however, is that the effect of surface tension begins to be important precisely for wavenumbers $k \sim 0.01$. Therefore the maximum for the bounded case (dashed line) is larger than that for the unbounded case (dotted line). This feature is present over the entire range $100 \leqslant \Gamma_v \leqslant 10^4$ that we have explored.

There is an intrinsic viscous lengthscale of the perturbation problem which appears in the argument of the Airy functions,

$$l = \left(\frac{2\pi}{Re_v\, k}\right)^{\frac{1}{3}}.$$

In the example of figure 4, this quantity becomes of order one for $k \sim 1$. Predictably, for wavelengths in this range or shorter, the bounded and unbounded results are close.

In the next figure we show the effect of Re_v on the growth rate of the first (continuous lines) and second (dotted lines) mode, again for $\Gamma_v = 1000$. Figure 5(*a*) is for the bounded case and figure 5(*b*) is for the unbounded case. The maximum is in all cases more pronounced for the bounded configuration and increases with the Reynolds number Re_v. The second mode is instead stabilized by an increase in the Reynolds number. For large k the growth rates for the bounded and unbounded cases

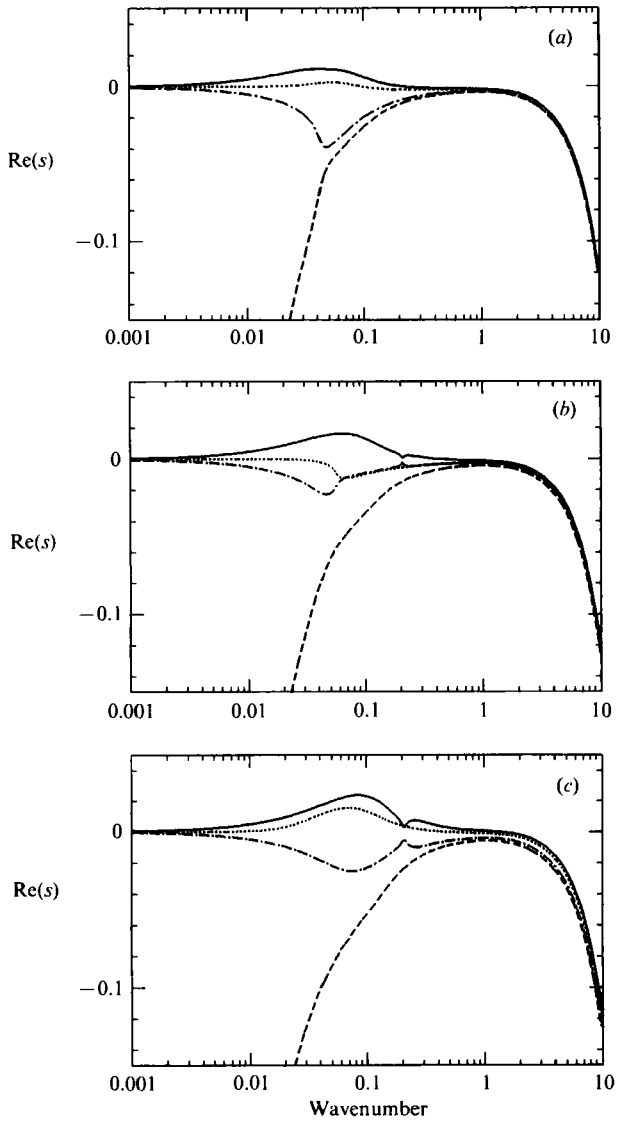

FIGURE 6. Dimensionless growth rate Re(s) *vs.* dimensionless wavenumber k for the four surface modes of the air film problem. —, $s^{(+)}$; · · · · ·, $s^{(0)}$; · · — · —, $s^{(-)}$; — — —, $s^{(1)}$. $Re = 1$, $Ca = 10^{-3}$. (*a*) $\alpha = \frac{1}{16}$; (*b*) $\alpha = \frac{1}{4}$; (*c*) $\alpha = \frac{3}{4}$.

tend to coincide, and decrease proportionally to k^2, which seems to be at variance with a statement of Hinch's (1984).

6. Results

We now return to the complete problem posed in §3 and discuss several examples on the basis of the models of the previous two sections. The numerical results to be described have been obtained from the stream-function formulation (38)–(42) by means of a standard shooting technique (see e.g. Keller 1968; Drazin & Reid 1981).

The present problem is characterized by three dimensionless parameters, the Reynolds number, the capillary number, and α. Within the context of the model

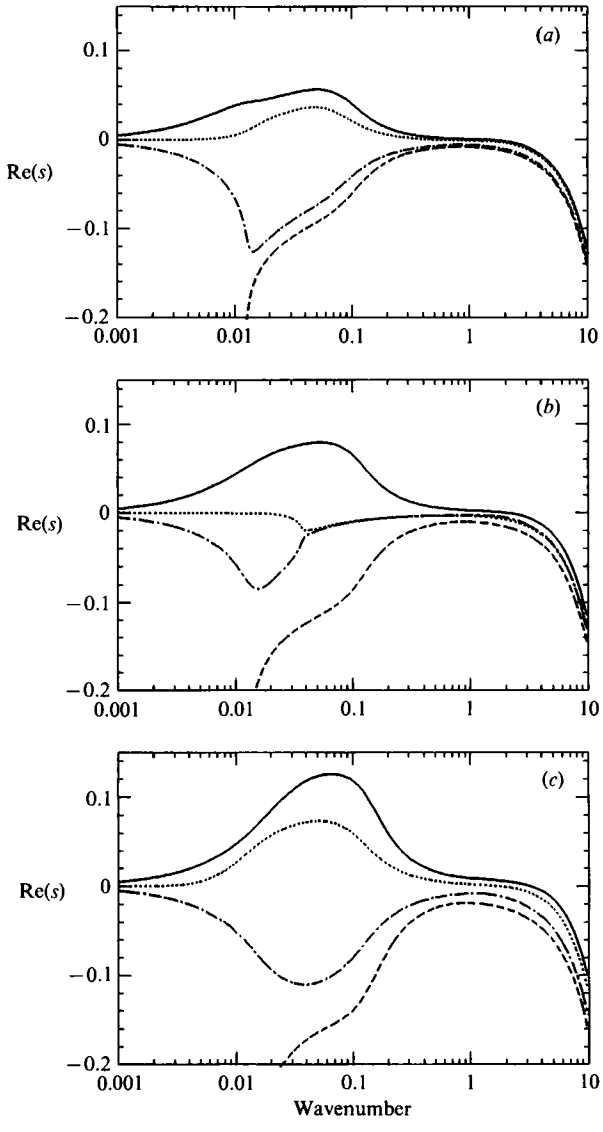

FIGURE 7. As in figure 6, with $Re = 10$, $Ca = 10^{-3}$.

assumed in this study, for a given gas–liquid combination, only the entrainment velocity W_f and film thickness $2d$ can be prescribed arbitrarily. Furthermore, as has already been remarked, it is very likely that a relation exists between these two quantities in the actual physical process, so that in an experiment only the entrainment velocity could be selected arbitrarily. However, in view of the incomplete understanding of the process that we have at present, we shall discuss our results treating Re, Ca, and α as independent quantities. In this way, a better insight into the mechanisms underlying the instability can be gained.

Figures 6–8 show the growth rate, Re (s), of the four surface modes $s^{(+)}$ (continuous line), $s^{(-)}$ (dash-and-dot line), $s^{(0)}$ (dotted line), and $s^{(1)}$ (dashed line) for several different combinations of the parameters Re, Ca, and α chosen so as to span a region of physical interest in parameter space. For some of these cases, figure 9 shows the

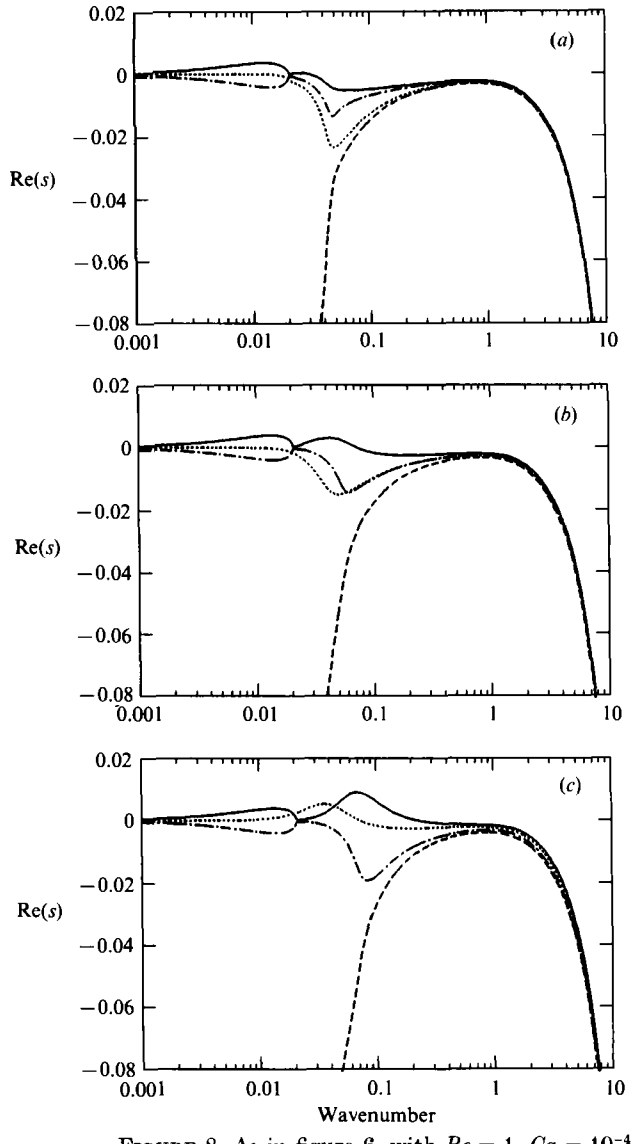

FIGURE 8. As in figure 6, with $Re = 1$, $Ca = 10^{-4}$.

phase velocity $-\mathrm{Im}\,(s)/k$, which is however of lesser interest for the study of the instability. Further results of this type can be found in Lezzi (1990). In the graphs the wavenumber ranges between 10^{-3} and 10. The density ratio ϵ is held fixed, equal to 1.207×10^{-3}, which is the appropriate value for air–water at 20 °C. For the parameter α, which may be viewed as a dimensionless imposed pressure gradient opposing the entrainment process, we consider the values $\frac{3}{4}$, corresponding to zero net mass transport in the film, $\frac{1}{4}$, corresponding to the film thickness d_1 for which no stress is exerted on the right-hand liquid surface, and $\frac{1}{16}$, corresponding to a film thickness equal to $\frac{1}{2}d_1$. For the air–water case at 20 °C, when W_ℓ ranges between 0.1 and 2 m s^{-1}, the Reynolds number varies between 0.06 and 5.7 for $\alpha = \frac{1}{4}$, while Ca increases from 2.5×10^{-5} to 5×10^{-4}. Therefore, we consider the values 10^{-1}, 1, and 10 for the Reynolds number and the values 10^{-4} and 10^{-3} for the capillary number.

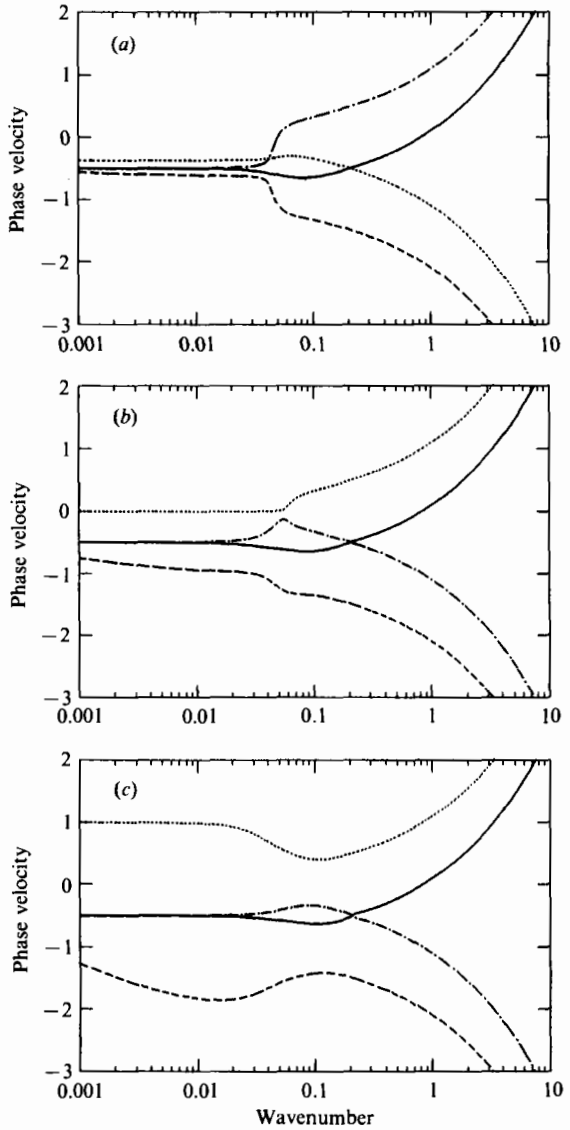

FIGURE 9. Dimensionless phase velocity *vs.* dimensionless wavenumber k for the four surface modes of the air film problem for the cases of figure 6.

The growth rate exhibits a striking variety of behaviours and a clear sensitivity to the parameters α and Re. For all values of α and Ca, an increase in the Reynolds number greatly enhances the instability. For the least-stable mode $s^{(+)}$, for given Re and Ca, an increase in α is destabilizing, while, for all modes, a decrease in Ca has a stabilizing influence. Since the instability is driven by the downward-moving liquid on the left of the film, and is inhibited by viscosity (all the more effective the thinner the film) and surface tension, qualitatively these trends are as expected. For a fuller understanding of the results, however, it is useful to compare them with those of the preceding two sections.

For the purposes of the following discussion, it is convenient to divide the range of wavenumbers in three different regions. We consider a long-wavelength region,

where $k < 10^{-2}$, corresponding to wavelengths at least two orders of magnitude longer than the film thickness. Here, the Kelvin–Helmholtz instability plays an important role. Wavelengths of order of the film thickness or smaller form another region corresponding to the wavenumber range $1 \leqslant k$. Here, the viscous instability mechanism for unbounded fluids is important. In the intermediate interval of wavenumbers, which is the most important since it is here that the eigenvalues attain their maximum in most cases, the dominant physical process seems to be the viscous instability as modified by the presence of a boundary.

6.1. *Kelvin–Helmholtz instability*

From the asymptotic analysis of §4, it is known that the modes $s^{(\pm)}$ tend toward the two modes of the Kelvin–Helmholtz instability at long wavelengths. Although we expected the Kelvin–Helmholtz model to be a good approximation for the film down to wavelengths about an order of magnitude longer than the film thickness, the numerical solutions show that its domain of validity is substantially smaller. Equation (49) is found to approximate the curves $s^{(\pm)}$ within 10% in the long-wavelength region previously defined, i.e. for $k < 10^{-2}$.

The two eigenvalues $s_{\mathrm{KH}}^{(\pm)}$ given by (49) are purely imaginary for k greater than a critical wavenumber k_{c} given by $\frac{1}{4}Re\,Ca/\epsilon$, whereas the absolute value of the real part attains its maximum at $k_{\mathrm{M}} = \frac{2}{3}k_{\mathrm{c}}$. Furthermore, the Kelvin–Helmholtz eigenvalues do no depend on the parameter α.

Figure 10(*a–c*) shows a detailed comparison between the numerical results $s^{(\pm)}$ (continuous lines) and the long-wavelength approximation (dashed lines). In figure 10(*a*), the value of $Re\,Ca$, 10^{-5}, is such that the critical wavenumber for the Kelvin–Helmholtz instability, k_{c}, lies in the long-wavelength region. It is seen that in this case one can use k_{M} to obtain a reliable estimate of the wavenumber of one of the relative maxima of the growth rate for $s^{(+)}$. In general, however, as in this example, this value does not necessarily coincide with the most unstable wavelength.

For the cases of figure 10(*b* and *c*), for which $Re\,Ca = 10^{-3}$ and 10^{-2}, the critical wavenumber for the Kelvin–Helmholtz instability has moved to the intermediate- and short-wavelength regions, respectively. In these cases it is seen that the Kelvin–Helmholtz model looses its validity at wavenumbers much smaller than k_{M} and becomes useless, except for one interesting vestige. When k_{c} falls in the intermediate region (figure 10*b*), two local small, but sharp dips interrupt the smoothness of $s^{(+)}$ and $s^{(-)}$. These structures occur near the value of k_{c} where the real part of $s_{\mathrm{KH}}^{(\pm)}$ rapidly vanishes. Other than this, it is apparent that the behaviour of the curves $s^{(\pm)}$ is determined by mechanisms quite different from the velocity jump across the film.

6.2. *Viscous instability*

As discussed in §5, the viscous instability arises from a viscosity discontinuity and is controlled by the shear rate in the viscous fluid. In the present problem there are two such discontinuities, and therefore we shall compare the results of the complete model with two sets of results for the viscous instability. In this comparison, care must be exerted because of the different velocity units used in the scalings of §§3 and 5. The correspondence that preserves the dimensional shear rate at the left-hand interface is readily seen to be

$$Re_{\mathrm{v}} = W_\ell' Re,$$

where

$$W_\ell' = \frac{\mathrm{d}W}{\mathrm{d}x}(-1) = \frac{1+4\alpha}{2}. \tag{64}$$

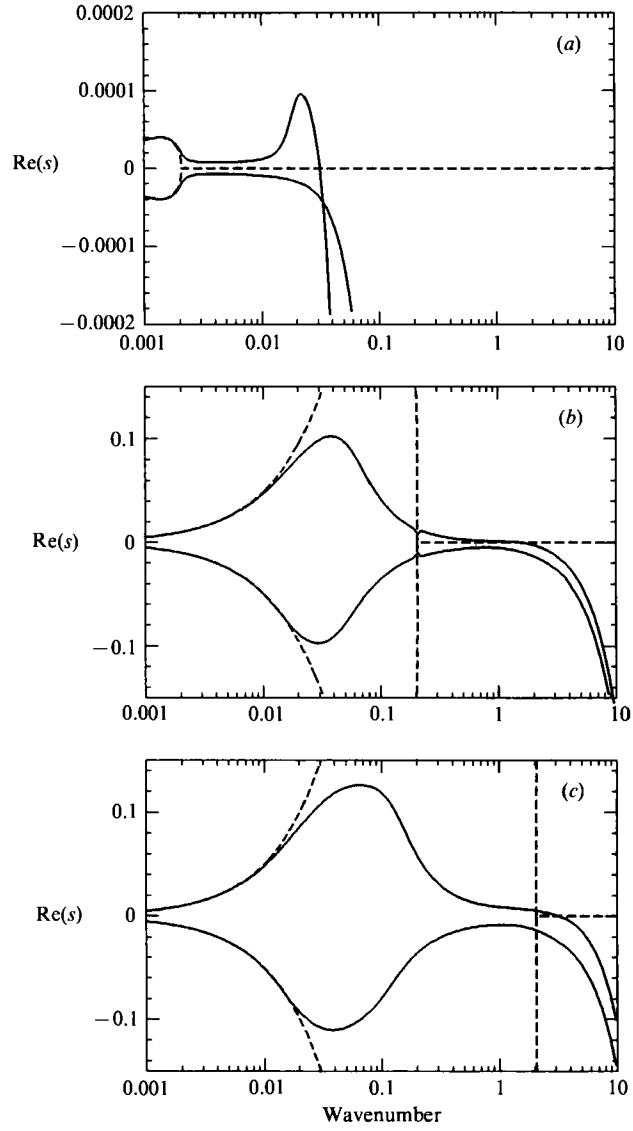

FIGURE 10. Comparison of the growth rates for the modes $s^{(\pm)}$ as given by the complete model (——) with the modes $s^{(\pm)}_{\mathrm{KH}}$, equation (49), of the Kelvin–Helmholtz, long-wavelength approximation (– – –). (*a*) $Re = 0.1$, $Ca = 10^{-4}$, $\alpha = \frac{3}{4}$, $k_c = 2.07 \times 10^{-3}$; (*b*) $Re = 10$, $Ca = 10^{-4}$, $\alpha = \frac{3}{4}$, $k_c = 2.07 \times 10^{-1}$; (*c*) $Re = 10$, $Ca = 10^{-3}$, $\alpha = \frac{3}{4}$, $k_c = 2.07$. k_c is the wavenumber at which the Kelvin–Helmholtz eigenvalues become purely imaginary. The maximum of $s^{(+)}_{\mathrm{KH}}$ occurs for $k = \frac{2}{3}k_c$.

Similarly, for the right interface,

$$Re_{\mathrm{v}} = |W'_{\mathrm{r}}|\,Re,$$

with

$$W'_{\mathrm{r}} = -\frac{\mathrm{d}W}{\mathrm{d}x}(1) = -\frac{1-4\alpha}{2}. \tag{65}$$

Here we use the modulus because W'_{r} is negative for $\alpha < \frac{1}{4}$. This causes no difficulties since, as pointed out in §5, the real part of the roots of (58) and (63) are invariant under inversion of the flow direction.

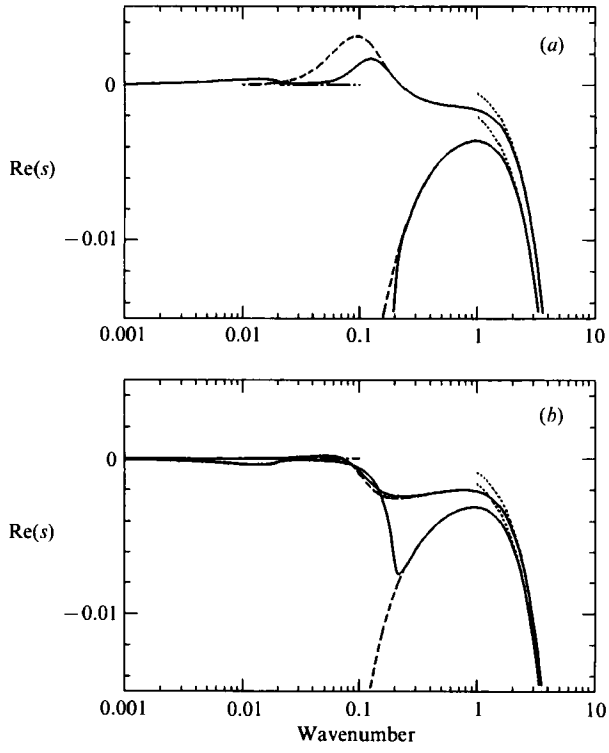

FIGURE 11. Comparison of the growth rates for the modes (*a*) $s^{(+)}$, $s^{(1)}$, and (*b*) $s^{(0)}$, $s^{(-)}$ as given by the complete model (——) with the corresponding modes of the short-wavelength approximations for the bounded (– – –) and unbounded (· · · · ·) configurations. The dash-and-dot line indicates the long-wavelength, Kelvin–Helmholtz approximation $s_{\mathrm{KH}}^{(\pm)}$, equation (49). Here $Re = 0.1$, $Ca = 10^{-3}$, $\alpha = \frac{3}{4}$.

In addition, to preserve the value of the dimensional surface tension coefficient σ in the film and in the model problems, the value of the parameter Γ_{v} must be selected according to the relation

$$\Gamma_{\mathrm{v}} = \frac{Re}{Ca}.$$

In figures 11–13 we consider two representative cases in detail. In figures 11 and 12 the continuous lines show the results for the complete problem, while the dashed lines and the dotted lines are the results for the viscous bounded and unbounded models, respectively. Figures 11(*a*) and 12(*a*) show the growth rates for the modes $s^{(+)}$ and $s^{(-)}$ associated with the left-hand interface, while figures 11(*b*) and 12(*b*) are for the modes $s^{(0)}$ and $s^{(-)}$ corresponding to the right interface. It can be seen in figures 11(*a*) and 12(*a*) that the first two modes for $Re_{\mathrm{v}} = W_{\ell}' Re$ give a good approximation to the roots $s^{(+)}$ and $s^{(1)}$ of the complete problem, while, from figures 11(*b*) and 12(*b*), those corresponding to $Re_{\mathrm{v}} = |W_{\mathrm{r}}'| Re$ are close to the roots $s^{(0)}$ and $s^{(-)}$. For the viscous stratification model with an unbounded viscous fluid, it is found that the approximation is accurate only for short wavelengths. However, for a configuration with a finite layer of viscous fluid having a thickness equal to that of the air film and bounded by a rigid wall, the agreement extends to the intermediate-wavelength region as well. The physical explanation for this result was given in §5 and hinges on the very small density of the air with respect to the liquid. To check

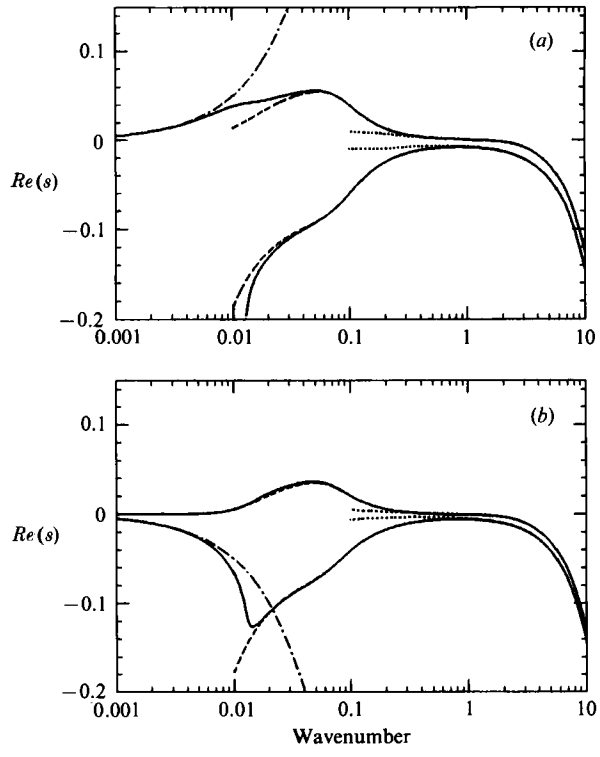

FIGURE 12. As in figure 11, with $Re = 10$, $Ca = 10^{-3}$, $\alpha = \frac{1}{16}$.

this explanation, we have studied a few cases corresponding to equal densities, $\epsilon = 1$. As expected, agreement between the results for the viscosity-stratification model and the complete problem then disappears.

As the parameter α varies between 0 and $\frac{3}{4}$, the shear rates W'_ℓ and W'_r range between $\frac{1}{2}$ and 2, and $-\frac{1}{2}$ and 1, respectively. For any value of α, $Re_v = W'_\ell Re$ is larger than $Re_v = |W'_r| Re$. Since, as was pointed out in §5, the higher Re_v the larger the growth rate, the mode $s^{(+)}$ associated with the left-hand interface is always less stable than the mode $s^{(0)}$ corresponding to the right-hand interface.

The phase velocity for the modes $s_{KH}^{(\pm)}$ is opposite to that induced by the viscous stratification mechanism. A further illustration of the limited validity of the Kelvin–Helmholtz mechanism and of the dominant role played by the viscosity stratification can therefore be obtained from a consideration of the phase velocities of the interfacial waves. Figure 13 (*a*, *b*) shows these velocities for the modes $s^{(+)}$ and $s^{(1)}$ for the two cases of figures 11 and 12. A similar transition between the two controlling mechanisms can be easily discerned in many of the examples of figure 9.

7. Summary and conclusions

Our analysis shows that only the two modes $s^{(+)}$ and $s^{(0)}$ have an unstable range of wavelengths. The $s^{(+)}$ mode is always the less stable of the two. For this mode, the instability is controlled to varying degrees by the Kelvin–Helmholtz mechanism and by the viscosity stratification. Only the latter mechanism seems to play a role for the other unstable mode.

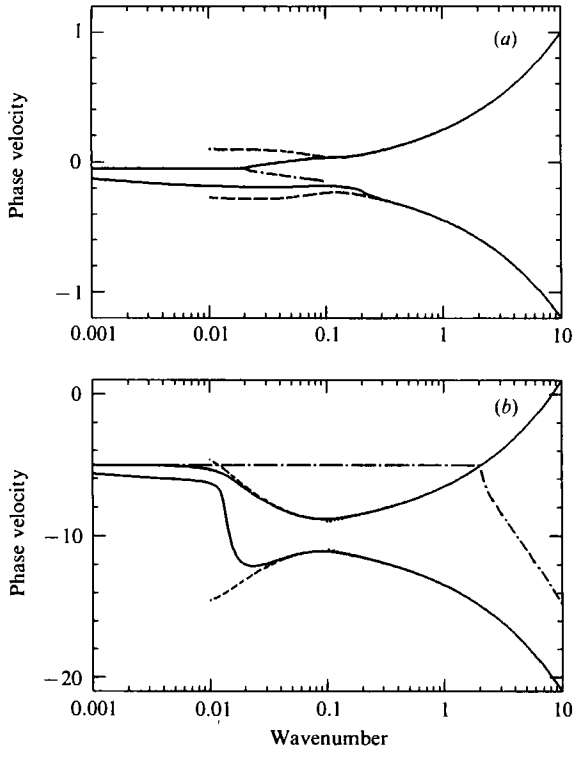

FIGURE 13. Phase velocities of the modes $s^{(+)}$, $s^{(1)}$ for the cases of (*a*) figure 11, and (*b*) figure 12. ——, Air film results; ·–·–·, Kelvin–Helmholtz mode $s_{KH}^{(+)}$; – – –, viscosity stratification model, bounded configuration; · · · · ·, viscosity stratification model, unbounded configuration.

When the critical value k_c for the Kelvin–Helmholtz instability falls in the long-wavelength region $k < 10^{-2}$, the real part of $s^{(+)}$ has two separate maxima. The first one peaks at around the most unstable wavelength for the Kelvin–Helmholtz instability. The second one is found for intermediate wavelengths and is due to the viscosity stratification. It is almost negligible for small values of the dimensionless pressure gradient α but, as α increases, it becomes of comparable magnitude and then larger than the first maximum.

When, by changing the product $Re\,Ca$, k_c is shifted to intermediate wavelengths, the mode $s^{(+)}$ tries to 'interpolate' between the two mechanisms (see figures 11*a* and 12*a*), until the two maxima merge with a resulting peak somewhere between $k \sim 0.01$ and $k \sim 0.1$. This maximum is substantially smaller than that predicted by the Kelvin–Helmholtz theory for the same parameter values.

Also the real part of the mode $s^{(0)}$ displays a broad maximum in the same range of wavenumbers except when α is close to $\frac{1}{4}$. This value corresponds to zero shear rate at the right interface, for which the viscous mechanism is shut off. The maximum becomes more and more pronounced as $|W_r'|$ (defined in (65)) increases, but it never grows larger than the maximum of the other mode. For those combinations of the parameters for which $s^{(+)}$ exhibits two maxima, the $s^{(0)}$ peak lies between them. In these cases the air film possesses three distinct preferred disturbances.

In addition to the air film problem, we have studied in §5 a situation in which the viscous layer is in a state of linear shear flow and one of the boundaries is either absent or substituted with a rigid, no-slip one. The results indicate that most of the

important features of the complete air film problem are reproduced by these simpler models owing to the large density difference between the air and the liquid.

We have also considered a variant of the air film problem in which the unperturbed parabolic velocity profile (7) is retained, but one of the two interfaces is substituted by a rigid, no-slip wall. Depending on which interface is replaced, either the pair $s^{(+)}$, $s^{(1)}$ or the peak $s^{(0)}$, $s^{(-)}$ disappears, as expected. However, the results for the remaining modes are only slightly affected, an indication of their relative independence of the nature of the other boundary and the details of the unperturbed velocity field. The controlling parameter seems to be the value of the shear at the interface.

The picture that we have summarized corresponds to the case in which the fluid in the film has a much smaller density than the other fluid, which is the situation of interest in the air entrainment problem that has motivated the present investigation. From a limited study of cases in which the two fluids have a comparable density, we have found that the viscosity stratification model reproduces the complete results only in the limit of very short wavelengths, for which the two interfaces are essentially uncoupled.

The results described in this paper show the importance of viscosity in the dynamics of the model that we have studied. However, our account of viscous effects has been incomplete insofar as the viscosity of the liquid has been neglected. It might be objected, therefore, that the final status of our conclusions remains open to question, if only on logical grounds. While we do not have a fully satisfactory answer to this objection, we may make the following remarks. Essentially, one can expect two type of effects from the viscosity of the liquid. The first one arises from the presence of a non-zero shear rate in the liquid. Since, as is clear from (1), this shear rate is smaller than that in the gas by a factor of the order of $\mu_a/\mu_\ell \ll 1$, one would expect only minor consequences to arise from the neglect of this quantity. The second effect is the damping of the instabilities that we have found. If one were to estimate this effect by using the damping constant of gravity–capillary waves, $2\nu_\ell k^2$, one would find a negligible correction except for the lowest Reynolds number case that we have considered, 0.1, where the maximum growth rate may be predicted to decrease by up to 50%. The applicability of this estimate is however not obvious in the present case in view of the presence of a non-zero stress applied to the liquid surface by the air layer. In any event, it is found experimentally that the length of the air film increases with the viscosity of the liquid (cf. e.g. figure 1 with figure 13 of Lin & Donnelly 1966). This finding seems to indicate that liquid viscosity will dampen but not suppress the instability. In view of this result, the destabilizing mechanisms that have been our primary concern in this study seem therefore to remain relevant to the mechanics of the actual physical process.

As a final point we may apply the previous numerical results to the jet entry example of figure 1. Since the film thickness is not available, we cannot go beyond an estimate of orders of magnitude. The water jet velocity is approximately 0.7 m/s, which gives $Ca = 1.8 \times 10^{-4}$. With $d = 30$ μm, the Reynolds number (6) has the value 1.4 and the timescale used in the non-dimensionalization is $\rho_a d^2/\mu_a \approx 6 \times 10^{-5}$ s. A typical order of magnitude of the dimensionless growth rates shown in figures 6 and 8 is 10^{-2}. With a jet velocity of 0.7 m/s, we thus predict a film length of the order of 0.4 cm, i.e. less than one jet diameter. This is in rough agreement with what is observed in the photo.

The authors are grateful to Dr J. H. Duncan for permitting them to reproduce one

of his photos in figure 1, and to Dr M. L. Banner and Dr D. Cato for giving them a videotape showing their remarkable visualization of the entrainment process in a laboratory breaking wave. Thanks are also due to Dr M. K. Smith for several helpful discussions and to the referees for some suggestions. This study has been supported by the Ocean Acoustics Program of ONR.

Appendix

We now give some details about the asymptotic analysis of §4. Let us first consider the case $\lim_{k\to 0} s \neq 0$. If we consider the relative order of magnitude of the terms in (25), we find that, in the limit $k\to 0$, $k\hat{O}(\hat{w}) = O(\hat{u}')$. Therefore, if we expand $\hat{w}$ as

$$\hat{w}(x,k) = w_0(x) + w_1(x)\,k + w_2(x)\,k^2 + \ldots, \tag{A 1}$$

the appropriate expansion for $\hat{u}$ is

$$\hat{u}(x,k) = u_c + k[u_0(x) + u_1(x)\,k + \ldots], \tag{A 2}$$

where u_c is a constant. Next, consider the limit of (30) and (31) as $k\to 0$. The right-hand sides are asymptotic to $\mp s u_c/\epsilon k$, which cannot be balanced by any term on the left-hand sides. Hence $u_c = 0$, i.e. $\hat{u} = O(k)$. Furthermore, from (32) and (33) we deduce that, to leading order, $\hat{\eta}_{\ell,r}$ are of order k at most. Accordingly, we set

$$\hat{\eta}_{\ell,r}(k) = k(a_{\ell,r0} + a_{\ell,r1}\,k + \ldots).$$

Substituting into (25) to (27) the previous expansions, together with

$$s(k) = s_0 + s_1\,k + s_2\,k^2 + \ldots,$$

$$\hat{p}(x,k) = p_0(x) + p_1(x)\,k + p_2(x)\,k^2 + \ldots,$$

and collecting terms multiplied by the same power of k, we obtain at the zeroth order

$$u_0' + \mathrm{i} w_0 = 0, \tag{A 3}$$

$$p_0' = 0, \tag{A 4}$$

$$w_0'' - s_0\,w_0 = 0, \tag{A 5}$$

with boundary conditions

$$w_0(\mp 1) = 0, \tag{A 6}$$

$$p_0(\mp 1) = \mp\frac{s_0}{\epsilon} u_0(\mp 1), \tag{A 7}$$

$$Re\, u_0(\mp 1) = s_0\, a_{\ell,r0}. \tag{A 8}$$

The general solution for w_0,

$$w_0 = A_0 \exp(s_0^{\frac{1}{2}} x) + B_0 \exp(-s_0^{\frac{1}{2}} x), \tag{A 9}$$

satisfies the boundary conditions $w_0(\mp 1) = 0$ if and only if $\sinh(2s_0^{\frac{1}{2}}) = 0$, from which the spectrum given in (45) follows.

For n odd, the solution of (A 5) is

$$w_0^{(n)} = A^{(n)} \cos(\tfrac{1}{2} n\pi x), \quad n = 1, 3, 5, \ldots,$$

while, for n even,

$$w_0^{(n)} = A^{(n)} \sin(\tfrac{1}{2} n\pi x), \quad n = 2, 4, 6, \ldots.$$

Once w_0 has been evaluated, u_0, p_0, $a_{\ell 0}$, and a_{r0} are readily calculated. When n is odd they are

$$u_0^{(n)} = -\mathrm{i}\frac{2A^{(n)}}{n\pi}\sin(\tfrac{1}{2}n\pi x),$$

$$p_0^{(n)} = \mathrm{i}\frac{n\pi A^{(n)}}{2\epsilon}(-1)^{n-1/2},$$

$$a_{r0}^{(n)} = -a_{\ell 0}^{(n)} = \mathrm{i}\frac{8\,Re\,A^{(n)}}{n^3\pi^3}(-1)^{n-1/2},$$

whereas, for n even,

$$u_0^{(n)} = -\mathrm{i}\frac{4A^{(n)}}{n\pi}\sin[\tfrac{1}{4}n\pi(x+1)]\sin[\tfrac{1}{4}n\pi(x-1)],$$

$$p_0^{(n)} = 0,$$

$$a_{\ell,r0}^{(n)} = 0.$$

When s vanishes as $k \to 0$ we use the expansion (46). The same expansions (A 1) and (A 2) with $u_c = 0$ as before hold in this case also. Making use of these results in the second of (26), we deduce that $\hat{p}' = O(k)$ so that

$$\hat{p}(x,k) = p_c + k[p_0(x) + p_1(x)\,k + \ldots],$$

with p_c a constant which, from (30), is seen to vanish. After this preliminary analysis, expand $\hat{\eta}_\ell$ and $\hat{\eta}_r$ as

$$\hat{\eta}_{\ell,r}(k) = a_{\ell,r0} + a_{\ell,r1}\,k + a_{\ell,r2}\,k^2 + \ldots,$$

to find the zeroth-order approximation to our problem

$$u_0' + \mathrm{i}w_0 = 0, \tag{A 10}$$

$$u_0'' = p_0', \tag{A 11}$$

$$w_0'' = 0, \tag{A 12}$$

together with

$$w_0(\mp 1) = -W'(\mp 1)\,a_{\ell,r0}, \tag{A 13}$$

$$p_0(-1) = -\frac{s_0 - \mathrm{i}Re}{\epsilon}u_0(-1) + 2[u_0'(-1) - \mathrm{i}W'(-1)\,a_{\ell 0}], \tag{A 14}$$

$$p_0(1) = \frac{s_0}{\epsilon}u_0(1) + 2[u_0'(1) - \mathrm{i}W'(1)\,a_{r0}], \tag{A 15}$$

$$Re\,u_0(-1) = (s_0 - \mathrm{i}Re)\,a_{\ell 0}, \tag{A 16}$$

$$Re\,u_0(1) = s_0\,a_{r0}. \tag{A 17}$$

The general solution of the system (A 10)–(A 12) is

$$u_0(x) = -\mathrm{i}[AW(x) + Bx] + C,$$

$$w_0(x) = AW'(x) + B,$$

$$p_0(x) = -\mathrm{i}AW'(x) + D,$$

where A, B, C, and D are integration constants. By imposing the boundary conditions, after some manipulation, we end up with the following linear system:

$$[\mathrm{i}(s_0 - \mathrm{i}Re)^2 - \epsilon Re\,W'(-1)]\,a_{\ell 0} + [\mathrm{i}s_0^2 + \epsilon Re\,W'(1)]\,a_{r0} = 0, \tag{A 18}$$

$$-[s_0 - \mathrm{i}Re\,W'(1)]\,a_{\ell 0} + [s_0 - \mathrm{i}Re\,W'(1)]\,a_{r0} = 0, \tag{A 19}$$

which has non-trivial solutions only if its determinant vanishes. This condition yields the three roots

$$s_0^{(\pm)} = \frac{1}{2}\left[\mathrm{i} \pm \left(1 - 8\mathrm{i}\frac{\alpha\epsilon}{Re}\right)^{\frac{1}{2}}\right] Re,$$

$$s_0^{(0)} = \mathrm{i}\, Re\, W'(1).$$

From (A 19), it is clear that when $s_0 = s_0^{(\pm)}$, $a_{\ell 0}^{(\pm)}$ is equal to $a_{\mathrm{r}0}^{(\pm)}$. Then

$$A^{(\pm)} = -a_{\mathrm{r}0}^{(\pm)}, \quad B^{(\pm)} = 0,$$

$$C^{(\pm)} = \frac{s_0^{(\pm)}}{Re} a_{\mathrm{r}0}^{(\pm)}, \quad D^{(\pm)} = \left[\frac{(s_0^{(\pm)})^2}{\epsilon Re} + \mathrm{i}W'(1)\right] a_{\mathrm{r}0}^{(\pm)}.$$

If $s_0 = s_0^{(0)}$, we define

$$r_0 = \frac{Re\, W'(1) + \mathrm{i}\epsilon}{Re\, W'(-1) - \mathrm{i}\epsilon}.$$

Then, from (A 17), it follows that

$$a_{\ell 0}^{(0)} = -\frac{W'(1)}{W'(-1)} r_0\, a_{\mathrm{r}0}^{(0)},$$

and

$$A^{(0)} = W'(1)\frac{1 + r_0}{W'(1) - W'(-1)} a_{\mathrm{r}0}^{(0)},$$

$$B^{(0)} = W'(1)\frac{r_0 W'(1) + W'(-1)}{W'(1) - W'(-1)} a_{\mathrm{r}0}^{(0)},$$

$$C^{(0)} = \mathrm{i}[W'(1)]^2 \frac{1 + r_0}{W'(1) - W'(-1)} a_{\mathrm{r}0}^{(0)},$$

$$D^{(0)} = -[W'(1)]^2 \left[\frac{Re}{\epsilon} + \mathrm{i}\frac{1 + r_0}{W'(1) - W'(-1)}\right] a_{\mathrm{r}0}^{(0)}.$$

Note that, for $\alpha = \frac{1}{4}$, $W'(1)$ vanishes together with $a_{\ell 0}^{(0)}$, $u_0^{(0)}$, $w_0^{(0)}$ and $p_0^{(0)}$.

The first-order correction to $s^{(0)}$ in (48),

$$s_1^{(0)} = (1 - 16\alpha^2)\left[\frac{Re}{30} + \frac{\epsilon + \mathrm{i}2\alpha Re}{(1 + 16\alpha^2) Re - \mathrm{i}8\alpha\epsilon}\right] Re,$$

has been calculated by determining and solving the first-order problem for the unknown s_1, u_1, w_1, p_1, and $a_{\ell,\,\mathrm{r}1}$, for the case $s_0 = s_0^{(0)}$. The calculations have been carried out by using the algebraic manipulation package MACSYMA, a trademark of Symbolics, Inc.

REFERENCES

BANNER, M. L. & CATO, D. H. 1988 Physical mechanisms of noise generation by breaking waves – a laboratory study. In *Sea Surface Sound* (ed. B. R. Kerman), pp. 429–436. Kluwer.

BENJAMIN, T. B. 1957 Wave formation in laminar flow down an inclined plane. *J. Fluid Mech.* **2**, 554–574.

BIRIKH, R. V., GERSHUNI, G. Z. & ZHUKHOVITSKII, E. M. 1966 On the spectrum of perturbations of plane parallel flows at low Reynolds numbers. *J. Appl. Math. Mech.* **29**, 93–104.

CHANDRASEKHAR, S. 1961 *Hydrodynamic and Hydromagnetic Stability*. Clarendon.

DRAZIN, P. G. & REID, W. H. 1981 *Hydrodynamic Stability*. Cambridge University Press.

GUTHRIE, R. I. L. & BRADSHAW, A. V. 1969 The stability of gas envelopes trailed behind large spherical cap bubbles rising through viscous liquids. *Chem. Engng Sci.* **24**, 913–917.

HESLA, T. I., PRANCKH, F. R. & PREZIOSI, L. 1986 Squire's theorem for two stratified fluids. *Phys. Fluids* **29**, 2808–2811.

HINCH, E. J. 1984 A note on the mechanism of the instability at the interface between two shearing fluids. *J. Fluid Mech.* **144**, 463–465.

HNAT, J. G. & BUCKMASTER, J. D. 1976 Spherical cap bubbles and skirt formation. *Phys. Fluids* **19**, 182–194.

HOOPER, A. P. & BOYD, W. G. C. 1983 Shear-flow instability at the interface between two viscous fluids. *J. Fluid Mech.* **128**, 507–528.

HOOPER, A. P. & BOYD, W. G. C. 1987 Shear-flow instability due to a wall and a viscosity discontinuity at the interface. *J. Fluid Mech.* **179**, 201–225.

JOSEPH, D. D., RENARDY, M. & RENARDY, Y. 1984 Instability of the flow of two immiscible liquids with different viscosities in a pipe. *J. Fluid Mech.* **141**, 309–318.

KELLER, H. B. 1968 *Numerical Methods for Two-Point Boundary-Value Problems*. Blaisdell.

KOGA, M. 1982 Bubble entrainment in breaking wind waves. *Tellus* **34**, 481–489.

LAMB, H. 1932 *Hydrodynamics*, 6th edn. Cambridge University Press.

LEZZI, A. M. 1990 Topics in free-surface flows. Dissertation, The Johns Hopkins University.

LIN, T. J. & DONNELLY, H. G. 1966 Gas bubble entrainment by plunging laminar liquid jets. *AIChE J.* **12**, 563–571.

LONGUET-HIGGINS, M. S. & TURNER, J. S. 1974 An 'entraining plume' model of a spilling breaker. *J. Fluid Mech.* **63**, 1–20.

RAJARATNAM, N. 1967 Hydraulic jumps. In *Advances in Hydroscience*, vol. 4, pp. 197–280. Academic.

RENARDY, Y. 1987 Viscosity and density stratification in vertical Poiseuille flow. *Phys. Fluids* **30**, 1638–1648.

RENARDY, Y. & JOSEPH, D. D. 1985 Couette flow of two fluids between concentric cylinders. *J. Fluid Mech.* **150**, 381–394.

SCHULTEN, Z., ANDERSON, D. G. M. & GORDON, R. G. 1979 An algorithm for the evaluation of the complex Airy functions. *J. Comput. Phys.* **31**, 60–75.

SMITH, M. K. 1990 The mechanism for the long-wavelength instability in thin liquid films. *J. Fluid Mech.* **217**, 469–485.

YIH, C.-S. 1963 Stability of liquid flow down an inclined plane. *Phys. Fluids* **6**, 321–334.

YIH, C.-S. 1967 Instability due to viscous stratification. *J. Fluid Mech.* **27**, 337–352.